Numerical Predictions on Fluid-Structure Bend-Twist Coupling of Wind Turbine Blades

M. Masoudi, K. Pope
Department of Mechanical Engineering
Memorial University of Newfoundland
St. John's, Canada
Email: mm6864@mun.ca, kpope@mun.ca

***Abstract*—In this paper, power enhancement potential of NREL Phase VI rotor with bend-twist coupling is investigated with new numerical predictions. Geometry based bend-twist coupling is introduced to an NREL Phase VI turbine through a curved planform for power enhancement purposes. Fluid-structure interaction analysis is performed on two configurations of the blade, for a range of wind speeds to determine the induced elastic twist. The CFD predictions are verified with experimental data from NREL wind tunnel testing of an S809 airfoil. Two blade designs, one with an L spar and the other with a box spar, are modelled and the elastic twist is compared. The results show better elastic twist properties from an L spar, which is 0.67˚ from a swept blade with 1.5 m bend depth. A 1.89% power improvement is calculated due to elastic twist using BEMT.**

***Index Terms*—fluid-structure interaction, bend-twist coupling, wind turbine blade**

I. INTRODUCTION

Modern large wind turbines benefit from active pitch control systems that add complexity and cost to the rotors. With active pitch control, the blades pitch around their axis to change the angle of attack and adjust to the wind conditions. However, smaller machines are typically fixed pitch and operate with simpler control methods. Fluctuations in wind speed results in a change in angle of attack that is no longer optimal. A passive adaptive blade twists as it bends to keep the optimum angle of attack. Stoddard [1] measured a 2.5˚ elastic twist in wind blades and suggested that elastic twist can be employed to improve performance.

Aeroelastic tailoring can be employed by coupling the twist of the section to the bending of the blade. Aeroelasting tailoring can be towards either power improvement or load alleviation. Calculations by Malcolm [2], Lobitz [3] and Verelst [4] indicate fatigue load reduction by employing bend-twist coupling (BTC). Berry [5] reported a 2.4 to 8.6% reduction in bending load with a 4˚ elastic twist. By discussing optimal pre-twist in blades, Cappuzi [6] stated that elastic twist can be employed to bring section twist angles closer to their optimal design value. Blade pre-twist is not optimal but is a suitable compromise over all operating conditions. Bend twist coupling can be achieved through material and geometry selection. An example of geometry BTC is a swept blade, as illustrated in Fig. 1. In a curved design, the load applied on the sections that are off the pitch axis, creates a pitching torque, which results in an elastic twist [7]. Tests on a full scale Sweep-Twist Adaptive Rotor (STAR) showed a reduction in operating loads allowing for larger blades [8, 9]. A 12% increase in energy capture was reported by increasing the diameter by 10% while keeping the loads at the same level [8, 9]. A novel design by Capuzzi [10, 11] employed both material and geometry BTC for better results.

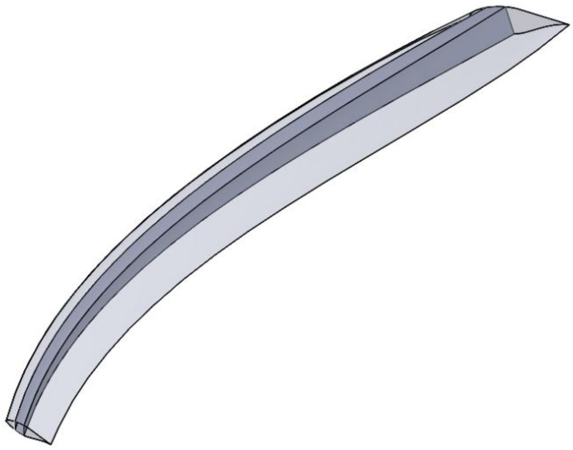

Figure 1. Swept blade with box spar.

In fixed pitch blades, as the wind speed increases, the angle of attack increases resulting in a non-optimal value for blade sections. By twisting the blade to a more optimal angle, it is possible to improve the power output. In this paper, geometry BTC is employed to enhance power of an NREL Phase VI wind turbine.

II. OPTIMIZED ELASTIC TWIST

The forces applied on an airfoil are illustrated in Fig. 2. Blade Element Momentum Theory is used on NREL Phase VI blades to derive blade section torque and power equations. The section force component $\delta F = L\,Sin\varphi - L\,Cos\varphi$ that creates torque around the rotor axis is shown in Fig. 2. Lift and drag forces can be obtained from Equation (1) and Equation (2) where C_l is the lift

Manuscript received May 31, 2018; revised May 2, 2019.

doi: 10.18178/ijmerr.8.4.506-510

coefficient, C_d is the drag coefficient, L is the lift force, D is the drag force, ρ is the air density, W is the relative wind velocity, and A is the section area.

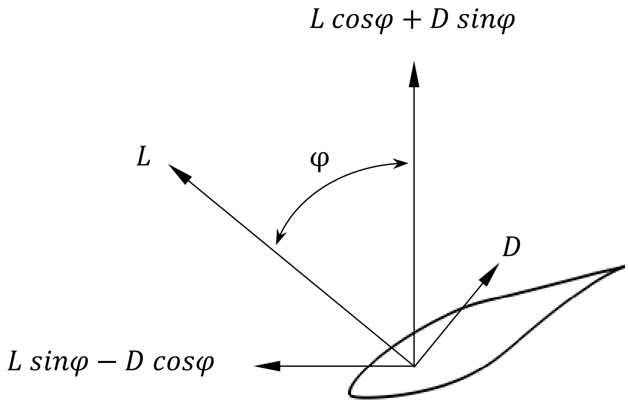

Figure 2. Aerodynamics of a typical blade (modified from [12]).

$$C_l = \frac{2\ L}{\rho\ W^2\ A} \quad (1)$$

$$C_d = \frac{2\ D}{\rho\ W^2\ A} \quad (2)$$

Substituting L and D into force component δF , for a section of blade provides

$$\delta_F = \frac{1}{2}\ \rho\ W^2 \delta A\ (C_l\ sin\ \varphi - C_d\ cos\ \varphi) \quad (3)$$

The torque created from a section of the blade in distance r from the rotor axis is

$$\delta T = r \times \delta F \quad (4)$$

Substituting Equation (3) into Equation (4) gives an equation for a blade section torque

$$\delta_T = \frac{1}{2}\ \rho\ W^2 \delta A\ (C_l\ sin\ \varphi - C_d\ cos\ \varphi)\ r \quad (5)$$

Power is the product of torque by angular velocity

$$\delta_P = \delta_T \times \Omega \quad (6)$$

By substituting Equation (5) into Equation (6) an equation for the power of a section of the blade with the area of δA is developed.

$$\delta_P = \frac{1}{2}\ \rho\ W^2 \delta A\ (C_l\ sin\ \varphi - C_d\ cos\ \varphi)\ r \quad (7)$$

Power of the rotor now can be calculated by integrating δ_P over the span of the blade for both blades, where B is the number of blades and is maintained at 2.

$$P = B \int_{r_0}^{R} \delta_P \quad (8)$$

The torque equation is optimized and the optimal elastic twists are computed. As illustrated in Fig. 3, a nose down elastic twist is needed for optimal power at U = 10 m/s. A nose down twist is a counterclockwise twist angle based on the airfoil orientation presented in Figure 2.

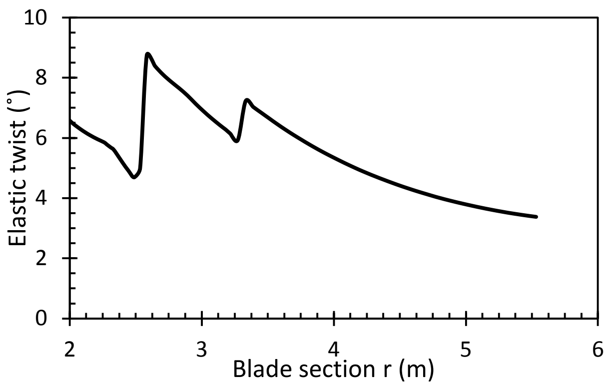

Figure 3. Optimal elastic twist for maximum power output at U = 10m/s.

III. Swept Blade

To form the curved planform of the blade, a power curve of order 4 is used and normalized to provide the desired bend depth at the tip. Bend depth is the perpendicular distance of the tip of the blade measured at 30% chord to the pitch axis of the blade. Two bend depths of 1 m and 1.5 m are studied. Figure 4 is the planform of the modified NREL Phase VI rotor blade. The blade data are extracted from [13]. The blade with a box spar is illustrated in Fig. 1.

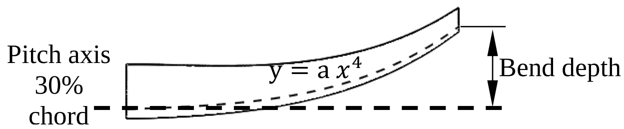

Figure 4. Modified curved blade planform.

IV. FSI Model

Ansys Mechanical and Fluent are employed to conduct one-way FSI analysis on the blade. CFD analysis is conducted to calculate the aerodynamic forces. The forces are passed to FE software to calculate the blade deformations. The deformed blade section angles are then calculated and subtracted from that of un-deformed blade to find the induced elastic twist for each blade section.

A. CFD

A C-grid is developed around the blade. The mesh is structured with hexahedral cells. A total quantity of 1,081,038 cells are used in the domain. The rectangular domain is illustrated in Fig. 5. To consider the rotation of the blade, an inlet velocity profile is implemented in Fluent such that the inlet boundary conditions have a linearly increasing y-velocity component that is in the plane of rotation perpendicular to the blade span. Figure 6 illustrates the wind relative velocity vector on different sections of the blade. Turbulence model $k - w$ is used as it has been widely used in the studies of wind turbine blades [14, 15].

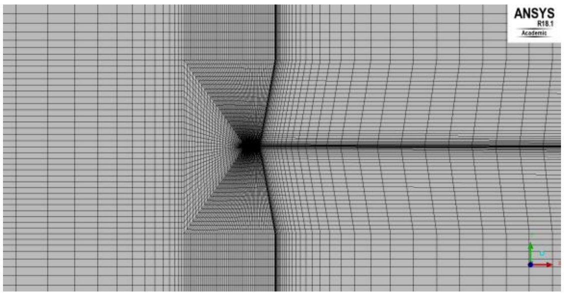

Figure 5. Rectangular domain with C-grid around the blade.

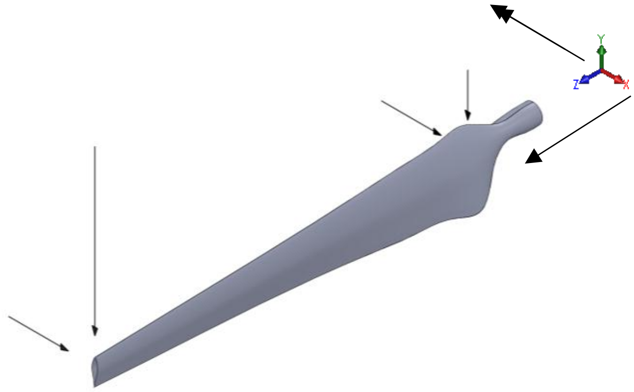

Figure 6. Velocity vectors on the blade.

B. FEM

The blade is meshed using 188,165 quadrilateral Shell 181 elements and 187,357 nodes. The blade mesh is illustrated in Figure 7. An equivalent material is used for the blade skin and spar. An elasticity modulus of $E = 1.56 \times 10^{10}$ Pa and Poisson's ratio of $\nu = 0.42$ are employed [16]. Blade skin has a constant thickness of 10^{-3} m and the spar thickness linearly decreases from 10^{-2} m at the root to 10^{-3} m at the tip. In the thicker model, the spar thickness is doubled. The rotational forces from the blade weight are applied on the blade. The resulting force is calculated from the rotational velocity and applied as a body force on the blade (to represent blade rotation).

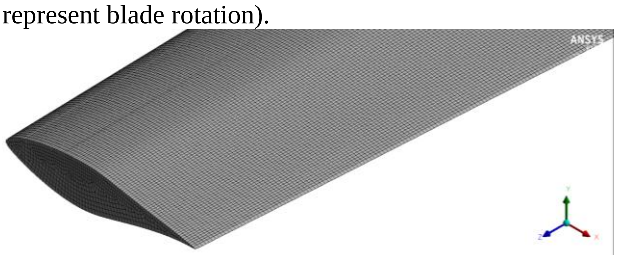

Figure 7. Blade mesh.

V. Results and Discussion

A. Grid Verification

The section at r = 4.275 m with Re = 10^6 for which experimental data are available is selected for verification. CFD mesh verification is done using the pressure coefficient around the section. Fig. 8 compares CFD results with experimental data. There is good agreement between CFD and experimental data in majority of the section, except for the very tip of the airfoil on the suction side where the CFD model underestimates the pressure.

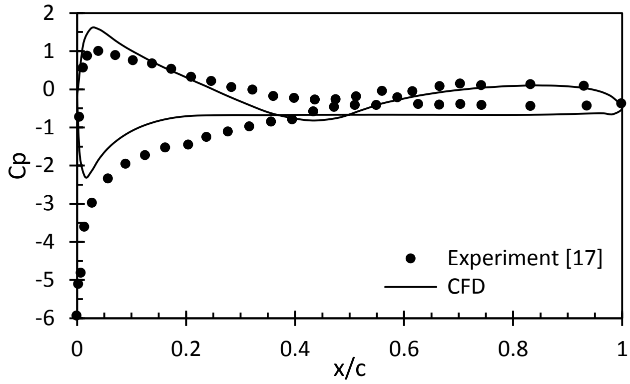

Figure 8. Coefficient of pressure for α = 15˚ at Re=1 million [17].

B. Elastic Twist and Power Increase

Figure 9 is a plot of deformed blade with contours of flapwise deformation in y direction. Darker color indicates more deflection at the tip. The diagonal contour lines are indications of induced twist for blade sections.

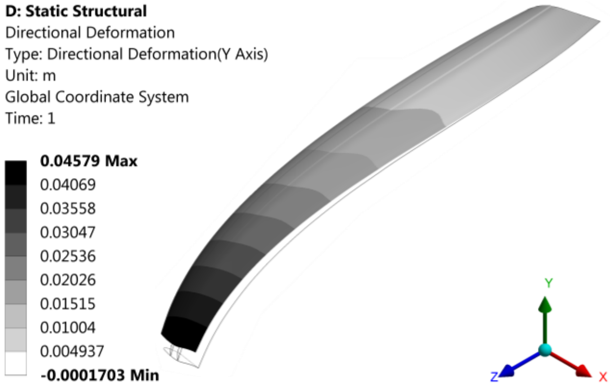

Figure 9. Flapwise bending of the blade with box spar at U_∞ = 15.

As illustrated in Fig. 10, induced elastic twist is greater at higher wind speeds. The effect of bend depth on elastic twist is presented in Fig. 11. Twist angle of up to 0.45˚ can be achieved with a bend depth of 1.5 m at a wind speed of 10 m/s. An average increase of 41% in elastic twist can be achieved with 50% increase in bend depth at the rated wind speed of 10 m/s. However, a blade with sharper curve planform is generally more expensive to build and the power gains might not offset the manufacturing costs. Elastic twist for a wind speed of 15 m/s is presented in Fig. 12. Elastic twist of up to 0.67˚ is predicted for a 1.5 m bend depth, at a wind speed of 15 m/s.

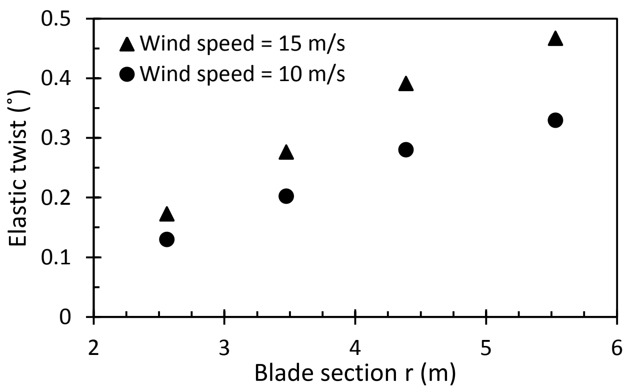

Figure 10. Induced twist of blade with L spar and bend depth of 1 m.

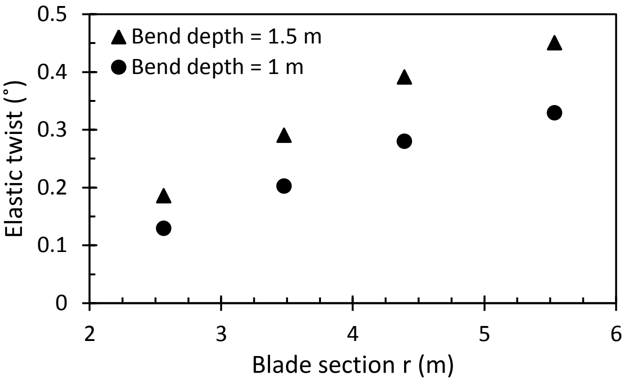

Figure 11. Induced twist of blade with L spar at U_∞ = 10 m/s.

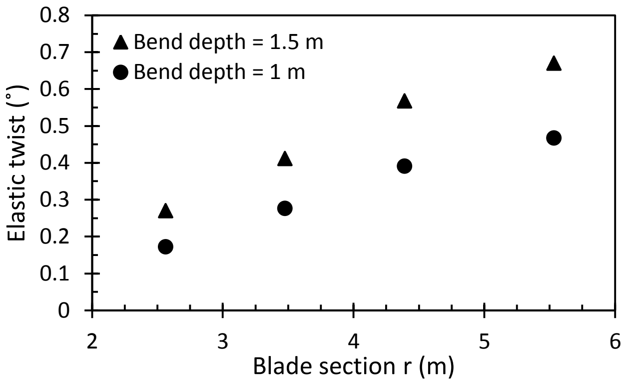

Figure 12.Induced twist of blade with L spar at U_∞ = 15 m/s.

As illustrated in Fig. 13, the blade with box spar has less elastic twist compared to a blade with L spar. A box spar allows for the formation of a shear flow circuit that will resist torsion and part of the torque resulting in less elastic twist. The advantage of using an L spar over a box spar is that the blade with L spar experiences 18% more elastic twist. However, from other design criteria, a box spar might have superiority as it provides more stability in vibrations during wind fluctuations. The blade with box spar experiences less flapwise deformation because a box spar has greater bending stiffness compared to an L spar which has a single shear web.

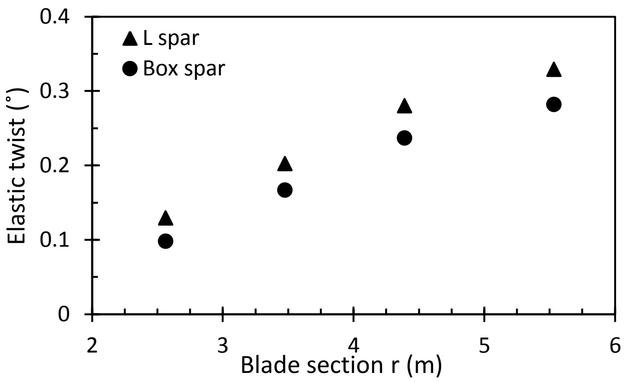

Figure 13. Induced twist for bend depth = 1 m at U_∞ = 10 m/s.

Based on these numerical predictions, the induced elastic twist and the rotor power is calculated. Equation 8 is numerically integrated and the power of the rotor is calculated. A 1.89% power improvement due to elastic twist is predicted for the blade with 1.5 m bend depth at the rated wind speed of 10 m/s.

VI. Conclusion

A modification to the NREL Phase VI blade was made to investigate swept blades with two different bend depths. Fluid-structure interaction analysis was performed at different wind speeds and the CFD results were verified with experimental data. The induced elastic twist of the blade at different sections were reported and a maximum elastic twist of 0.67˚ was predicted from a bend depth of 1.5 m for a wind speed of 15 m/s. A blade with box spar was developed to investigate the effects of a closed section spar on elastic twist. The study predicts that a blade with a box spar experiences 18% less elastic twist compared to a blade with an L spar. A 1.89% improvement is estimated due to elastic twist at 10 m/s wind speed.

Acknowledgements

The authors of this paper gratefully acknowledge the financial support of the Research and Development Corporation of Newfoundland and Labrador.

References

[1] F. Stoddard, V. Nelson, K. Starcher, and B. Andrews, "Determination of elastic twist in horizontal axis wind turbines (HAWTs)," Subcontract Report NREL/SR-500-12087, June 2006.
[2] D. J. Malcolm and A. C. Hansen, "WindPACT turbine rotor design study: June 2000-June 2002," Subcontract Report NREL/SR-500-32495, 2006.
[3] D. W. Lobitz and P. S. Veers, "Load mitigation with bending/twist-coupled blades on rotors using modern control strategies," *Wind Energy*, vol. 6, pp. 105-117, 2003.
[4] D. R. Verelst and T. J. Larsen, "Load Consequences when sweeping blades - a case study of a 5 MW pitch controlled wind turbine," Technical University of Denmark, Risø National Laboratory for Sustainable Energy, 2010.
[5] D. Berry and A. T., "Design of 9-meter carbon-fiberglass prototype blades: CX-100 and TX-100," *Sandia Report SAND2007-0201*, September 2007.
[6] M. Capuzzi, A. Pirrera, and P. M. Weaver, "A novel adaptive blade concept for large-scale wind turbines. Part I: Aeroelastic behaviour," *Energy*, vol. 73, pp. 15-24, 2014.
[7] M. D. Zuteck, "Adaptive Blade Concept Assessment: Curved Planform Induced Twist Investigation," Sandia National Laboratories SAND02-2996, Albuquerque, NM, 2002.
[8] T. D. Ashwill, "Passive Load Control for Large Wind Turbines," in 51st AIAA/ASME/ASCE/AHS/ASC Structures, Structural Dynamics, and Materials Conference, Orlando, FL, April 2010.
[9] T. D. Ashwill, G. Kanaby, K. Jackson and M. Zuteck, "Development of the Swept Twist Adaptive Rotor (STAR) Blade," in *Proc. 48th AIAA Aerospace Sciences Meeting*, Orlando, FL, 4-7 Jan 2010.
[10] M. Capuzzi, A. Pirrera, and P. M. Weaver, "A novel adaptive blade concept for large-scale wind turbines. Part II: structural design and power performance," *Energy*, vol. 73, pp. 25-32, 2014.
[11] M. Capuzzi, A. Pirrera and P. M. Weaver, "Structural design of a novel aeroelastically tailored wind turbine blade," *Thin-Walled Structures*, vol. 95, pp. 7-15, 2015.
[12] T. Burton, N. Jenkins, D. Sharpe, and E. Bossanyi, *Wind Energy Handbook*, West Sussex: Willey & Sons, 2011.
[13] M. M. Hand, D. A. Simms, L. J. Fingersh, D. W. Jager, J. R. Cotrell, S. Schreck and S. M. Larwood, "Unsteady Aerodynamics Experiment Phase VI: Wind Tunnel Test Configurations and

Available Data Campaigns," National Renewable Energy Laboratory NREL/TP-500-29955, December 2001.
[14] J. O. Mo and Y. H. Lee, "CFD Investigation on the aerodynamic characteristics of a small-sized wind turbine of NREL PHASE VI operating with a stall-regulated method," *Journal of Mechanical Science and Technology*, vol. 26, no. 1, pp. 81-92, 2012.
[15] N. N. Sørensen, J. A. Michelsen and S. Schrek, "Navier–Stokes predictions of the NREL phase VI rotor in the NASA Ames 80 ft×120 ft wind tunnel," *Wind Energy*, vol. 5, no. 2-3, pp. 151-169, 2002.
[16] K. Lee, Z. Huque, and R. H. S. E. Kommalapati, "Evaluation of equivalent structural properties of NREL phase VI wind turbine blade," *Renewable Energy*, vol. 86, pp. 796-818, 2016.
[17] R. R. Ramsay, J. M. Janiszewska, and G. M. Gregorek, "Wind Tunnel Testing of Three S809 Aileron Configurations for use on Horizontal Axis Wind Turbines, Airfoil Performance Report," *National Renewable Energy Laboratory NREL* , July 1996.

Mehdi Masoudi was born in Tehran, Iran in 1990. He moved to Canada in 2014 and lives in St. John’s, NL. Mr. Masoudi is a Master student of Mechanical Engineering (thermofluids and energy) in Memorial University of Newfoundland. Mr. Masoudi earned his Bachelor’s degree in Mechanical Engineering from KNTU in 2013.
His publications are: “Finite Element Analysis of Fir-tree Blade-disc Assembly”, Applied Mechanics and Materials Vol.392 (2013) 191-196 and “Effects of manufacturing tolerances on fatigue life of blades in a gas turbine”, 5th Conference on Rotating Equipment in Oil & Power Industries, Beheshti Intl. conference center, Tehran, Iran. Jan. 21-22, 2014. His current field of research is Renewable Energy, Wind Turbines and Fluid Structure Interaction. His previous research interests were Finite Element Modeling, Stress Analysis and Design of Structures. Mr. Masoudi is a member of the Canadian Society for Mechanical Engineering (CSME).

Kevin Pope is an Assistant Professor at Memorial University of Newfoundland. His research involves energy systems and multiphase flows. He is a member of the American Society of Mechanical Engineers, Canadian Society for Mechanical Engineering, and American Institute of Aeronautics and Astronautics. Dr. Pope is a recipient of the I. W. Smith Award from the Canadian Society for Mechanical Engineering.